



CHALMERS



Critical plane approach to low cycle thermal fatigue of welds in exhaust manifolds

Master's thesis in Applied Mechanics

JAKOB ALM

MASTER'S THESIS IN APPLIED MECHANICS

Critical plane approach to low cycle thermal fatigue of welds in exhaust
manifolds

JAKOB ALM

Department of Industrial and Materials Science
Division of Material & Computational Mechanics
CHALMERS UNIVERSITY OF TECHNOLOGY

Göteborg, Sweden 2018

Critical plane approach to low cycle thermal fatigue of welds in exhaust manifolds
JAKOB ALM

© JAKOB ALM, 2018

Examiner: Prof. Lennart Josefsson, Department of Industrial and Materials Science
Supervisor: Dr. Carl Sandström, Volvo Car Corporation

Department of Industrial and Materials Science
Division of Material & Computational Mechanics
Chalmers University of Technology
SE-412 96 Göteborg
Sweden
Telephone: +46 (0)31-772 1000

Cover:
Plastic strain amplitude in a solid submodel.

Chalmers Reproservice
Göteborg, Sweden 2018

Critical plane approach to low cycle thermal fatigue of welds in exhaust manifolds
Master's thesis in Applied Mechanics
JAKOB ALM
Department of Industrial and Materials Science
Division of Material & Computational Mechanics
Chalmers University of Technology

ABSTRACT

Components in internal combustion engines are often subjected to temperature cycling that lead to low-cycle fatigue due to thermal expansion and contraction. Furthermore, these thermal loads may be multiaxial and non-proportional in nature which means that traditional fatigue evaluation methods are not sufficient. Welds constitute another complication since they are often more sensitive to fatigue damage than the base material. This is in large part due to the notch effect associated with the boundaries of the weld in addition to the presence of tensile residual stresses near the weld.

At Volvo Cars, there is an interest in developing a new methodology for numerically evaluating the low cycle fatigue life of welds during thermal cycling. Methods that can account for non-proportional loading are of particular interest. One of the most prevalent methods for non-proportional multiaxial fatigue evaluation is the critical plane approach. Evaluating weld fatigue also requires treatment of the weld geometry to resolve the stress-strain gradients in the vicinity of the weld. This thesis explores the possibility of combining the critical plane approach with common weld modelling techniques to accurately model low cycle thermal fatigue. The Smith-Watson-Topper model using the maximum normal stress to the critical plane was chosen as the critical plane fatigue model and compared to a traditional strain-based fatigue evaluation methodology. Welds were modelled with shell elements, solid elements and with the effective notch method. Weld residual stresses were accounted for by considering them as a tensile mean stress combined with a mean stress correction. To assess and compare the methods, a welded exhaust manifold subjected to low cycle thermal fatigue was evaluated by using Finite Element Analysis (FEA).

It was shown that both the critical plane approach and traditional strain-based fatigue evaluation offered a conservative fatigue life estimate compared to available experimental values. It was also shown that modelling the weld with shell elements resulted in fatigue life estimates within the margin of error for the experimental values. Using the effective notch method gave the lowest fatigue life estimate but the fatigue failure location was predicted to be the weld toe which corresponded with known failure locations from experimental testing. Mean stress effects were shown to have a negligible impact at the considered fatigue lives. It is important to note that further numerical and experimental validation is needed before deploying the methodology in an industrial setting.

Keywords: Weld fatigue; Critical plane approach; Exhaust manifold; Low cycle fatigue; Thermal fatigue; Effective notch method

PREFACE

This master's thesis was done as the final part of my education at the master's programme Applied Mechanics during the spring of 2018. The project was carried out at the "Engine CAE - Solids" group within engine development at Volvo Car Corporation.

ACKNOWLEDGEMENTS

I would like to thank my supervisor Dr. Carl Sandström for his advice and overall knowledge about FEM, in addition to his good company during my stay at Volvo Cars. I would also like to thank my examiner Professor Lennart Josefsson for his guidance and vast knowledge about fatigue and welds. Thanks to Lena Johansson at Volvo Cars for providing me with information, test data and pictures from the thermal shock test. Additional thanks to the group manager Anders Thorell for allowing me to do my master's thesis with the group. Finally, I would also like to extend thanks to all of my coworkers for the warm welcome, overall advice and providing a pleasant working environment.

NOMENCLATURE

Acronyms

CFD	Computational Fluid Dynamics
FEA	Finite Element Analysis
HCF	High cycle fatigue
LCF	Low cycle fatigue
SWT	Swith-Watson-Topper
VCC	Volvo Car Corporation

Finite element method

C3D10	10-node tetrahedral solid element
C3D4	4-node tetrahedral solid element
S3	3-node triangular shell element
S4	4-node quadrilateral shell element

Continuum mechanics

σ	Cauchy stress tensor
ε	Strain tensor
\bullet_a	Amplitude of a quantity
$\Delta\bullet$	Range of a quantity
ε_n	Normal strain
\perp	Perpendicular to
σ_m	Mean stress
σ_n	Normal stress
σ_y	Yield strength
ε_e	Elastic strain
ε_p	Plastic strain
N_f	Number of cycles to failure
R	Stress ratio
S	Nominal stress
T	Temperature

Material parameters

α	Thermal expansion coefficient
ν	Poisson ratio
σ'_f	Fatigue strength coefficient
ε'_f	Fatigue ductility coefficient
b	Fatigue strength exponent
c	Fatigue ductility exponent
E	Young's modulus

Weld terminology

a	Throat size
t	Plate thickness
HAZ	Heat affected zone

CONTENTS

Abstract	i
Preface	iii
Acknowledgements	iii
Nomenclature	v
Contents	vii
1 Introduction	1
1.1 Purpose	1
1.2 Method	1
1.3 Scope and limitations	1
2 Theoretical framework	3
2.1 Material mechanics	3
2.2 Fatigue life prediction	5
2.3 Welded joints	6
2.4 Low cycle fatigue in welds	7
2.4.1 Local approaches	7
2.4.2 Critical plane approaches	8
3 Model: Exhaust Manifold X	9
3.1 Region weld A-B	9
3.2 Base finite element model	10
3.3 Global-local finite element model	11
3.4 Materials	11
3.5 Thermal analysis	12
3.6 Structural analysis	12
3.7 Contacts	13
4 Fatigue evaluation methodology	15
4.1 Weld modelling	15
4.1.1 Oblique shell elements	15
4.1.2 Solid elements	15
4.1.3 Solid elements with effective notch method	16
4.1.4 Weld evaluation	17
4.2 Damage models	17
4.2.1 Coffin-Manson damage model	17
4.2.2 Swith-Watson-Topper damage model	18
4.2.3 Mean stress effects	20
4.3 Statistical analysis of fatigue data	21
5 Results	23
5.1 Thermal analysis	23
5.2 Structural analysis	24
5.3 Fatigue	25
5.3.1 Oblique shell elements	26
5.3.2 Solid elements	26
5.3.3 Solid elements with effective notch method	27
5.3.4 Mean stress effects	27
6 Discussion	29
6.1 Error sources	29
7 Conclusions	31
7.1 Recommendations	31
Bibliography	33

1 Introduction

Welding is a common and effective metal joining method that is extensively used within the automotive industry in components ranging from panels to exhaust systems. However, welds are particularly susceptible to fatigue due to metallurgical changes from the welding process and the fact that boundaries of the weld acts as notches which raises the stress locally. In cars, it is common to weld components that would otherwise require expensive casting or forging processes to manufacture. For Volvo Car Corporation (VCC), a notable example would be Exhaust Manifold X, which is fitted to turbocharged petrol engines. The exhaust manifold and turbocharger is housed in a load bearing outer shell which is welded together from two sheet metal parts. Due to cyclic variations of temperature, the welded connections are subjected to thermal fatigue during the start-run-stop cycle of the engine. These fatigue loads are known to initiate cracks in the weld seams, whereby exhaust gases leak. This is detrimental to engine performance due to a loss of backpressure, in addition to heating the engine compartment. Furthermore, the leaked exhaust gases are not able to be filtered through a catalytic converter, which means that the vehicle is not able to maintain emission standards.

Currently, durability testing is performed on engine components in order to determine their durability under severe thermal loads. The main test is called a thermal shock test and consists of running the engine at maximum speed and then cooling it rapidly through forced convection, and repeating this for a specified amount of cycles. Since these tests may take several weeks to perform, it quickly becomes very expensive to perform design iterations if the exhaust manifold fails the durability test. Therefore, VCC perform Finite Element Analysis (FEA) of the engine components before any testing occurs, in order to ensure that the design of the engine components will withstand the loads. Currently, weld seams are modelled geometrically but evaluated using the same criteria as for the surrounding base material. Since fatigue cracks still occur in the welds despite prior FEA evaluation, it is clear that more sophisticated fatigue life evaluation methods are necessary.

1.1 Purpose

The purpose of the investigation is to evaluate new fatigue life evaluation methods that can account for the presence of welds, in addition to accounting for non-proportional multiaxial low cycle thermal fatigue. The aim is to provide answers to the following questions:

- Is it necessary to include the effects of non-proportional multiaxial loading to accurately estimate the fatigue life?
- What weld modelling method provides the best fatigue life estimate?
- What is the effect of including weld residual stresses in the fatigue life estimation?

1.2 Method

The difference between using simplified LCF methodology and more refined methods will be evaluated by studying an exhaust manifold named Exhaust Manifold X, which is known to have issues with weld fatigue. To this end, the thermal shock test on Exhaust Manifold X will be modelled by using FEA. Three different ways of geometrically modelling the weld geometry will be studied, together with two fatigue damage models. The fatigue models will be the Coffin-Manson model and the Swith-Watson-Topper (SWT) model with the critical plane approach. The FEA will be performed using ANSA 17.1.2 [1] as a preprocessor and ABAQUS Standard 2017 [2] as the solver. Postprocessing will be performed by using ABAQUS Viewer 2017 together with Python scripts that calculate certain key parameters, such as fatigue damage and fatigue life.

1.3 Scope and limitations

The fatigue assessment will be limited to low-cycle fatigue (LCF) due to extremely high temperature variations and resulting thermal stresses that will likely exceed the yield limit of the material. High cycle fatigue due to engine vibrations and other dynamic phenomena will not be considered. Creep-fatigue interactions will also not be considered. Residual stresses in the welds will not be modelled using FEA. Instead the influence of residual stresses will be accounted for by using a mean stress correction. No experimental testing will be performed.

2 Theoretical framework

The necessary theoretical framework for this investigation is presented in this chapter. The reader is expected to have basic knowledge of continuum mechanics, fatigue and the finite element method. Further details about continuum mechanics and fatigue can be found in Dowling [3] while Ottosen and Petersson [4] is an excellent reference for details about the finite element method.

2.1 Material mechanics

The mechanical response of virtually all metals may be described by a linear relationship, i.e Hooke's law, as long as the stresses are below the yield limit of the material. However if the material is stressed beyond the yield limit, the material will be subjected to irreversible plastic deformation and typically experience strain hardening. Figure 2.1 shows an example of loading beyond the yield limit σ_y where the material experiences strain hardening, followed by elastic unloading characterised by the elastic strain ε_e . After the elastic unloading, the plastic strain ε_p will remain in the material.

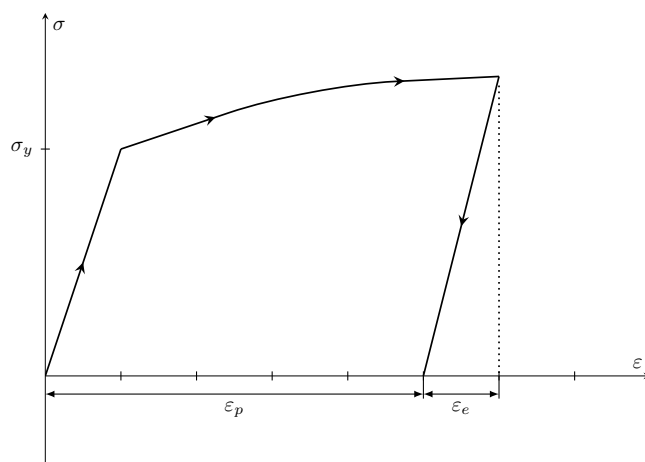


Figure 2.1: *Stress response of a strain hardening material and subsequent elastic unloading.*

In order to model strain hardening, it is necessary to implement a material model that accurately describes the behaviour of the material when the stress goes beyond the yield limit. For metals, the models are typically divided into isotropic hardening and kinematic hardening. Isotropic hardening is characterised by an uniformly expanding yield surface, while kinematic hardening is characterised by a yield surface that translates. Figure 2.2 shows an example of the evolution of a von Mises yield surface during biaxial loading for isotropic and kinematic hardening.

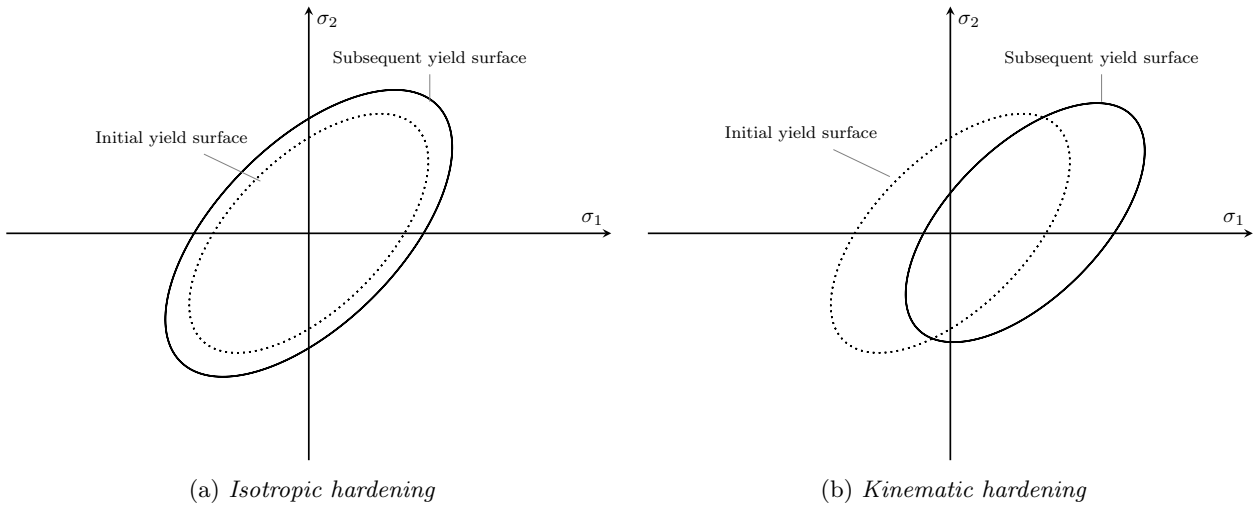


Figure 2.2: Yield surface evolution for isotropic and kinematic hardening when the load exceeds the yield limit.

Consider the case where the material is subjected to cyclic loading which causes the material to yield in each cycle. In that case, the material will ideally reach a stabilised state after a number of cycles. The stabilised state may either be elastic, in which case it's known as elastic shakedown, or it may be plastic in which case it's known as plastic shakedown. Plastic shakedown is characterised by closed plastic loop with a constant plastic strain amplitude in each cycle and no accumulation of plastic strain. However, it is possible that the material does not stabilise, whereby the plastic strain will accumulate in each cycle. This phenomena is called ratcheting and will rapidly lead to failure due to growing plastic deformation of the material. Ratcheting can be expected when there is a non-zero mean stress $\sigma_m \neq 0$ [5]. Figure 2.3 shows an illustration of ratcheting followed by a stabilised loop where plastic shakedown has occurred.

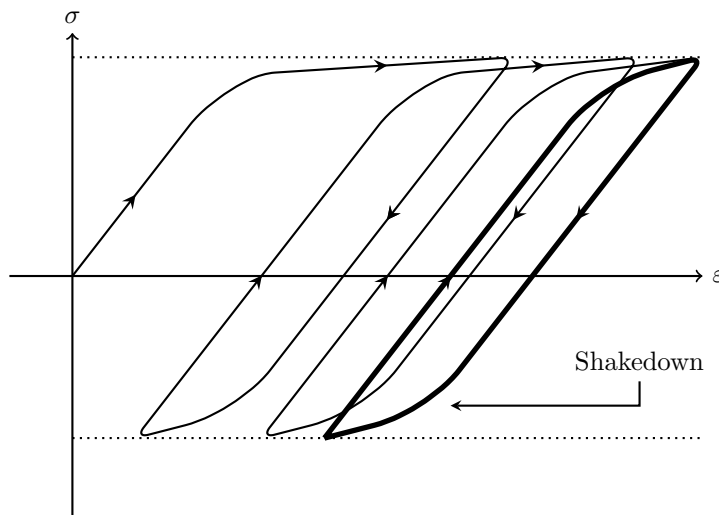


Figure 2.3: Illustration of plastic ratcheting followed by plastic shakedown. The stabilised loop can be seen in bold.

As one might infer from Figure 2.3, the isotropic hardening model cannot capture ratcheting since the yield surface location is fixed. Kinematic hardening can capture ratcheting and subsequent shakedown, although the complexity of the model will determine the accuracy. For example, linear kinematic hardening will predict plastic shakedown earlier than what occurs in reality. In principle, a non-linear kinematic hardening model is necessary to capture ratcheting. Commonly, the non-linear kinematic hardening is combined with linear isotropic hardening since most materials exhibit both expansion and translation of the yield surface during cyclic loading.

2.2 Fatigue life prediction

Materials have a tendency to experience crack growth during cyclic loading, even when the magnitude of the loads is well below the yield limit of the material. After a while the crack will grow to a critical length whereby the material will suddenly fail, often without any prior warning. This phenomenon is called fatigue, and accounts for a vast majority of structural failures [3]. The physical reason for fatigue failure is that microcracks initiate either in slip bands or between the grains of the material due to shear stresses on the microscale [6]. It is important to note that the stresses on the macroscale may be tensile, but they act as shear stresses on the microscale due to the random orientation of the grains. After the microcracks have grown sufficiently large, they propagate due to tensile stresses on the microscale. Crack growth due to tension is denoted mode I while crack growth due to in-plane shear and out-of-plane shear is referred to as mode II and mode III respectively. In most cases, crack growth occurs in mode I but there are cases in multiaxial loading where there are multiple modes of crack growth, so called mixed mode propagation.

In fatigue design, the most common tool is the Wöhler curve which is also known as the stress-life curve. In principle, a certain stress amplitude corresponds to a certain fatigue life. For HCF applications, one may also speak of a fatigue limit, where the fatigue life is infinite if the stress amplitude is below the fatigue limit. In LCF applications, it is usually more meaningful to study the strain since the stress-strain relationship is nonlinear in the plastic region. Similar to Wöhler curves, there exists strain-life curves that are modelled by the so called Coffin-Manson equation. Figure 2.4 shows typical Wöhler curves and Coffin-Manson curves for steel.

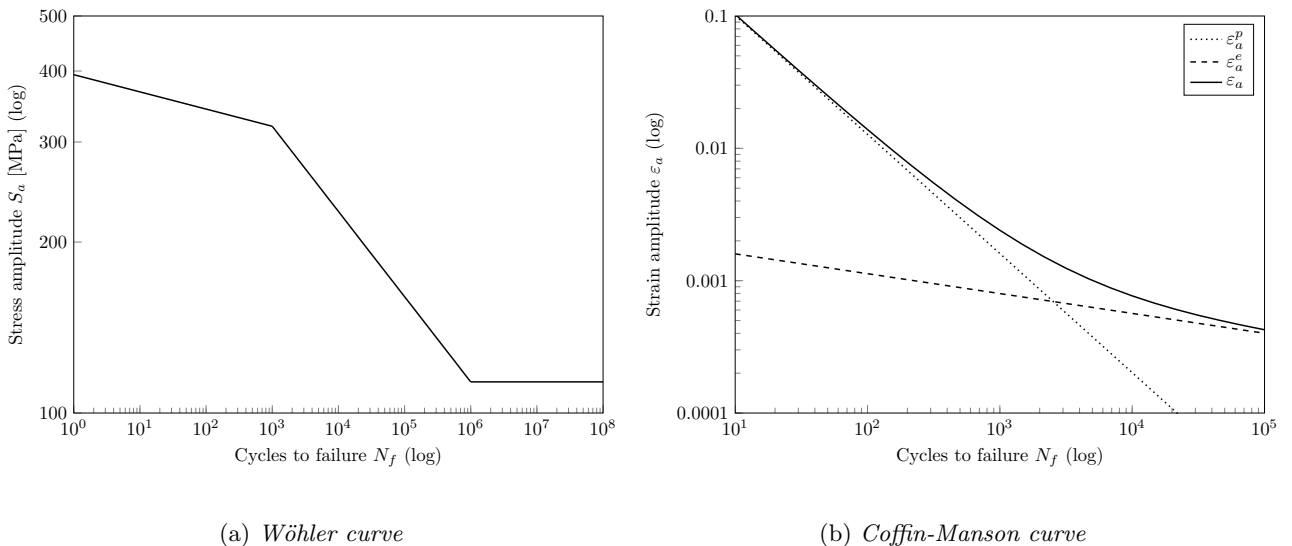


Figure 2.4: *Examples of design curves used in HCF and LCF design. Model data obtained from [7].*

For the Wöhler curve, the fatigue limit can clearly be seen at $N_f = 10^6$ cycles. In the Coffin-Manson curve, it is important to note that it is composed of two terms, namely the elastic and plastic portions. At very low fatigue lives, the elastic term can often be neglected as the plastic term will be dominant. Another important characteristic of the Coffin-Manson curve is the transition life N_t , where the elastic and plastic terms have equal influence on the fatigue life. Using Wöhler curves or Coffin-Manson curves is typically limited to uniaxial loading, since they are based on uniaxial testing. In some cases, it may be possible to extend their use to multiaxial loading by employing an equivalent stress-strain approach. However, that practice is limited to proportional multiaxial loading [6].

In the general case, multiaxial loading is non-proportional, where non-proportionality is defined by the principal directions changing direction during a load cycle [8]. If that is the case, an equivalent stress-strain approach is no longer valid. Figure 2.5 shows an example of proportional loading and non-proportional loading for the case of alternating normal strain ε_{xx} and shear strain γ_{xy} . For proportional loading, it is trivial to construct a shear range $\Delta\gamma$ and use with a corresponding fatigue model. In the case of non-proportional loading, the same task is non-trivial since there is no clear definition of a range.

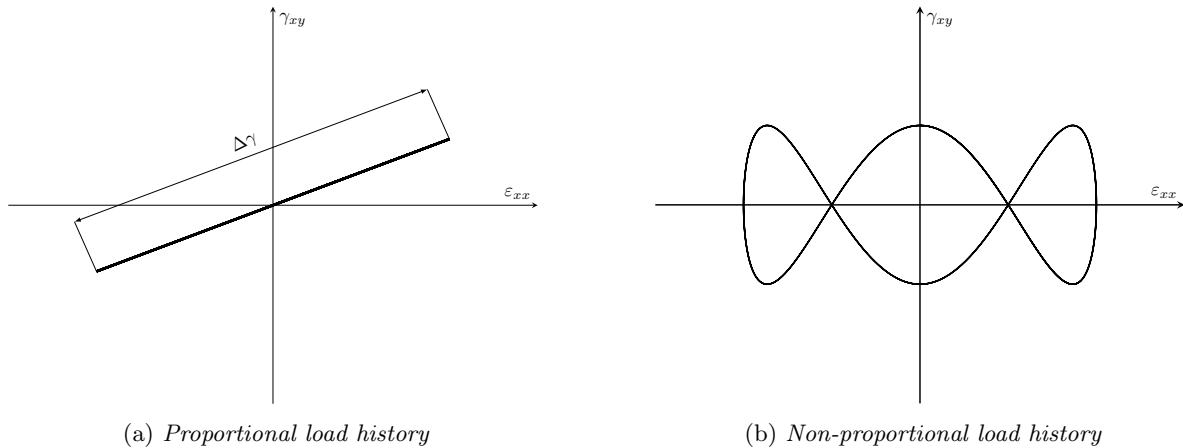


Figure 2.5: Example of proportional and non-proportional loading. For the non-proportional loading, the frequency of the shear strain is three times the frequency of the normal strain. Also, the shear strain is phase shifted 90°

The most common approach is to employ the so called *critical plane approach*, which is based on observations that fatigue cracks occur on either shear planes or normal planes of the material. To determine the fatigue life, candidate planes are generated for each material point, and the stress or strain state is projected onto each plane. The projection yields normal stresses/strains and shear stresses/strains on the plane which can be used to calculate pertinent damage parameters such as shear strain range $\Delta\gamma$ or normal stress range $\Delta\sigma_n$. By employing optimisation, the most damaging plane can be found. There exists various damage models that build on the critical plane approach and they are suitable for different types of fatigue problems since crack growth mechanisms can vary between materials. For example, the Swith-Watson-Topper model [9] is built on the hypothesis that crack growth occurs due to normal stresses and strains, while the Fatemi-Socie model [10] and the Brown-Miller model [11] hypothesise that crack growth occurs due to shear strain, with influences from normal stresses and strains. Since the different models predict different crack growth mechanisms which are material dependent, there is no model that can be expected to fit test data for any material [8].

2.3 Welded joints

Welding is a joining method for metals, which is based on applying heat to melt the base metal and a filler metal. The two metals are mixed and joined by fusion during cooling and subsequently form a joint that is typically stronger than the base material. Due to the fusion of the two metals, the local metallurgy of the welded structure is drastically changed. In general, the weld region can be divided into base metal, heat affected zone (HAZ) and weld metal. The HAZ is a region between the base metal and the welded joint which has changed metallurgical properties due to the intense temperature changes induced by the welding process. Figure 2.6 shows an example of a welded joint. It is called a transverse fillet weld or a lap joint. The weld joint, base metal and HAZ can be seen, in addition to the weld root and weld toe. In the case of fatigue loading, the weld toe and weld root are the most likely locations for crack initiation. This is mainly due to the material mismatch, brittle material behaviour of the weld zone and the geometrical discontinuities at the weld toe and root.

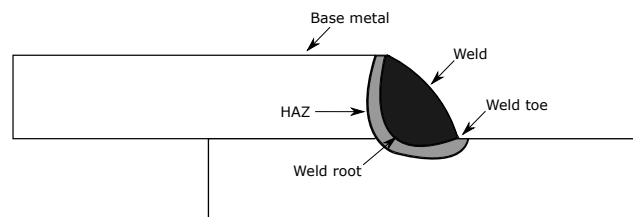


Figure 2.6: Illustrative example of a single transverse fillet weld, also called a lap joint.

During the welding process, the structure is subjected to high thermal strains due to uneven thermal

expansion of the material in the vicinity of the welded joint. Due to the extremely large temperature gradients, these thermal strains causes the material to yield locally. Therefore, tensile residual stresses are formed near the weld during the cooling process. In general, these residual stresses may be considered as a mean stress, which is well known to decrease or increase fatigue life depending on whether the stress is tensile or compressive. In design codes, this is usually accounted for by using Wöhler curves that are obtained directly from welded specimens, thereby including the effect of residual stresses and imperfections.

2.4 Low cycle fatigue in welds

One of the largest issues when studying weld fatigue are the difficulties associated with obtaining an accurate stress or strain field in the vicinity of the weld due to the geometrical discontinuity of the weld toe or weld root. In elastic calculations, the stress and strain will tend to infinity in the vicinity of sharp notches. An illustrative example of this notch effect can be seen in Figure 2.7.

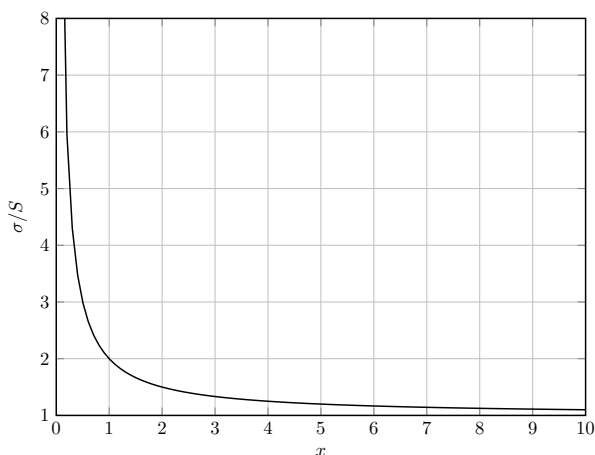


Figure 2.7: *Example of the notch stress phenomena. In this case, x is the distance from the notch, σ is the actual stress and S is the nominal stress away from the notch.*

It can be inferred that modelling the weld toe or weld root as a sharp notch will cause erroneous stress-strain fields, especially if the material model is purely elastic. Because of the difficulty associated with calculating the local stress-strain field in welds, the main focus of weld fatigue research has been to find methods that can determine the local stress-strain field. These methods are commonly called local approaches, and the most prevalent methods are the structural stress-strain method, the effective notch stress-strain method and the fracture mechanics approach [12]. While these methods were originally developed to calculate the HCF life of welds, there have been attempts to extend their applicability to LCF. The following section will briefly review some of the proposed methods from the literature.

2.4.1 Local approaches

The effective notch method together with equivalent strains was used by [13] to evaluate both HCF and LCF in fillet welded cruciform joints. In this paper, the authors resolved the geometrical discontinuities by modelling the weld toe and weld root with a given radius. Different radius values were used to determine the influence of the radius dimension on the estimated fatigue life. In addition, the author studied the influence of plate thickness and material mismatch. It was shown that a radius $\rho = 1$ mm resulted in most consistency compared to the experimental results. Furthermore, material mismatch was shown to have a significant impact on the low-cycle fatigue life of the weld.

Another possibility is to use a structural strain method as shown in [14]. In this article, the author reformulates the Battelle structural stress method [15] into a structural strain method. In short, membrane and bending stresses were evaluated from nodal forces and moments at a predefined distance from the weld toe. These stresses were then used to calculate membrane and bending strains which could be used to construct

a structural strain that represents the strain state in the weld toe. According to the author, the method is mesh-insensitive due to its reliance on forces and moments instead of stresses and strains. The suggested method showed good correspondence with the presented experimental data, but it was limited to weld toe failure and cases where the material was not fully plastic through the thickness. Furthermore, the author assumed that the material behaved perfectly plastic after yielding.

It is also possible to employ a fracture mechanics approach, where an initial crack is placed in the mesh and the resulting crack growth due to cyclic loading is calculated until a critical crack length is reached. By counting the number of cycles between the initial crack and the critical crack, it is possible to estimate the fatigue life of the material. This method was used by [16] together with a strain-based approach to calculate the fatigue life of butt welded specimens. The results were correlated to experimental data and it was shown that the approach gave very accurate results. One of the main limitations was that the author used a 2D mesh, which is generally not possible in industrial settings where entire systems are simulated. Employing a 3D mesh with similar density as the mesh used by the author would result in a large model and prohibitive computational cost.

All of the presented models showed good correspondence to the presented experimental values. The main flaw of the structural strain approach and the equivalent strain approach is that they condense the three-dimensional stress-strain state into a scalar value. Therefore, those methods are fundamentally incompatible with a critical plane approach where the entire stress or strain tensor is needed. The fracture mechanics approach would likely yield accurate fatigue life estimates but the required mesh size would be too small to be suitable for industrial applications.

2.4.2 Critical plane approaches

Critical plane approaches are not common when evaluating weld fatigue, especially with regard to LCF. However, there are a few examples for HCF in the literature. The critical plane approach with the Fatemi-Socie model was used by [17] to evaluate torsional fatigue in tubular weld joints considering the effects of residual stresses. The authors performed thermomechanical simulations of the welding process to generate a residual stress field, and then conducted a HCF analysis with the critical plane approach. Both the residual stress field and the fatigue life estimates were compared to experimental data. It was shown that the residual stresses moved the crack initiation position from the weld toe to a region away from the weld toe and beneath the surface. This was also the result from the experiments, where none of the specimens cracked from the weld toe.

The Fatemi-Socie model was also used in a similar fashion by [18] to evaluate high-cycle fatigue life in a pipe-to-plate fillet joint during multiaxial loading. The authors employed the effective notch method to model both the weld toe and the weld root. It was shown that the critical plane approach could provide adequate fatigue life estimates compared to data from 91 experimental tests. However, the authors did not account for residual stresses and they stress that the assessment procedure is still under development. Furthermore, they only evaluated the Fatemi-Socie damage parameter at the weld root, not at the two weld toe notches.

While none of the presented articles evaluated the low-cycle fatigue life of welds, it was still shown that the critical plane approach can be applied to welds with satisfactory results. Furthermore, both of the articles used the strain-based Fatemi-Socie model. Strain-based methods are typically used for LCF, therefore it is likely that the methodology could be extended to LCF. It was also shown that the critical plane approach can be combined with the effective notch method to produce reliable fatigue life estimates.

3 Model: Exhaust Manifold X

Exhaust Manifold X is an older version of exhaust manifold, made for use with turbocharged high performance petrol engines. The reason for using an older model is that newer versions are still under development and not suitable for publishing. Figure 3.1 shows the entire model with its respective components. Exhaust gases flow through the runners into the turbocharger, denoted scroll in the figure. After the turbocharger, the exhaust gases flow through the exit flange into the remaining exhaust system. The outer structural shell consists of an upper shell and a lower shell which are welded together along the midline. The main function of the outer structural shell is to house all the components, transfer loads and shield the engine compartment from heat. Flange 1-4 connect the exhaust manifold housing to the cylinder head through bolted connections.

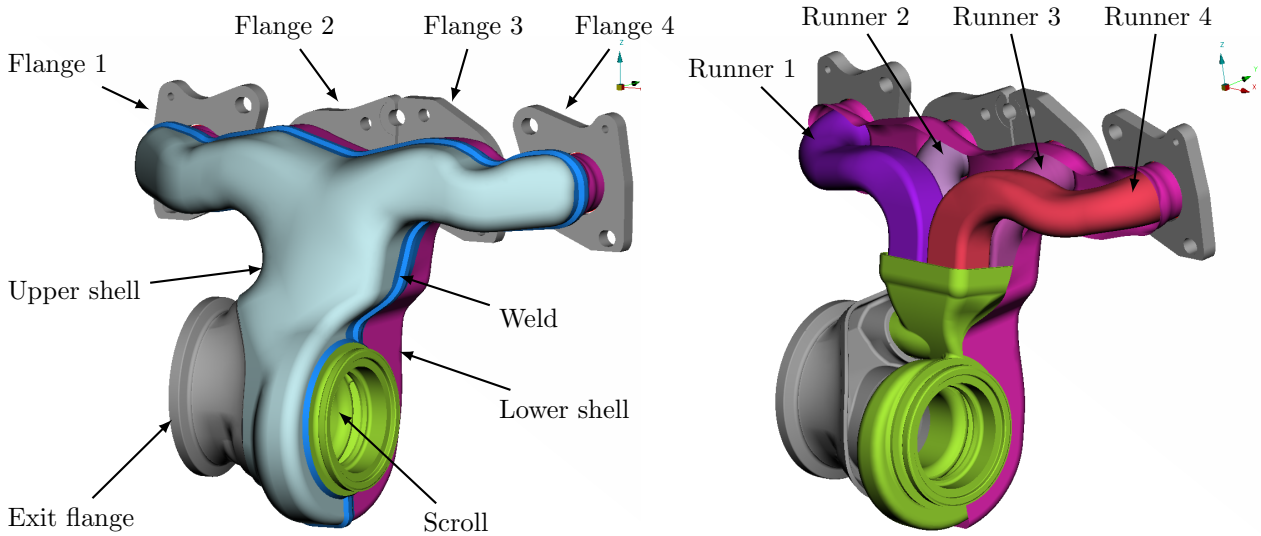


Figure 3.1: Full model of the exhaust manifold housing, including exit flange and turbine scroll.

It can be noted that the exhaust system, cylinder head and engine block has been omitted from the analysis. In real applications, these would have been included since the entire system is studied with respect to durability. However, that would have made the analysis too computationally expensive and therefore it was decided to only include the exhaust manifold subsystem and its corresponding components.

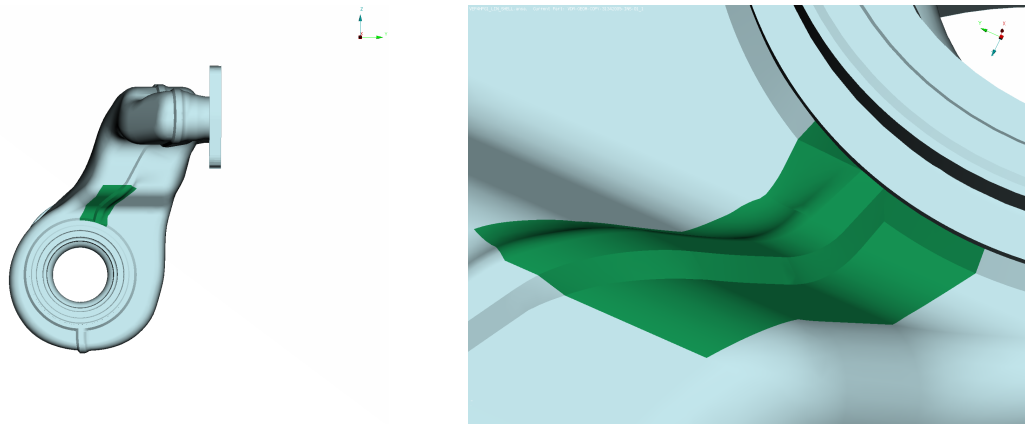
3.1 Region weld A-B

From testing at VCC, it was known that cracks tended to initiate in the weld toe of various weld seams during the thermal shock test. Figure 3.2 shows a weld toe crack in the weld that connects the scroll to the outer shell. It can be noted that the crack propagated along the weld toe, which is the expected behaviour for weld toe failure.



Figure 3.2: *Weld toe crack in a test engine after a thermal shock test.*

It was decided to focus the analysis on a region called weld A-B, due to the fact that cracks were known to occur there. Furthermore, it is a smaller region than the weld connecting the scroll to the outer shell. Therefore, the computational effort was reduced. In normal circumstances, weld seams are divided into categories depending on the weld geometry. Examples would be fillet welds and butt welds. In this case, the weld seam A-B could be considered as a combination of a lap joint and a misaligned butt joint. Figure 3.3 shows the region weld A-B and its location with respect to the entire exhaust manifold housing. As can be seen, the geometry of the region is quite complex due to the significant curvature that is present.



(a) *Location of region weld A-B in the global model*

(b) *Detailed view of region weld A-B*

Figure 3.3: *Region weld A-B highlighted in green*

3.2 Base finite element model

Sheet metal parts were modelled using mainly linear quadrilateral shell elements (S4), supplemented by triangular shell elements where necessary (S3). Cast or forged parts were modelled using linear tetrahedral elements (C3D4). Linear tetrahedral elements are known to be too stiff, but the effect of the overestimation was considered to be low. This is due to the fact that stresses and strains were not studied in any cast or forged parts. Welded connections were modelled in three different ways, which is described in more detail in Chapter 4.

3.3 Global-local finite element model

In order to study the region weld A-B in further detail, the so-called global-local approach was used. It is named global-local since the model is split into a global part that is usually modelled with a coarse shell mesh, while a local region of interest is modelled with a fine solid mesh. As with the base model, the global model used mainly S4 elements supplemented by S3 elements where necessary. The local region of interest used C3D10 elements, which are quadratic tetrahedral elements. Tetrahedral elements are usually not recommended, but it is easier to mesh complex geometries when using tetrahedral elements compared to hexahedral elements. Figure 3.4 shows the local zone with solid elements. As can be seen, the weld toe is a sharp notch in this model.

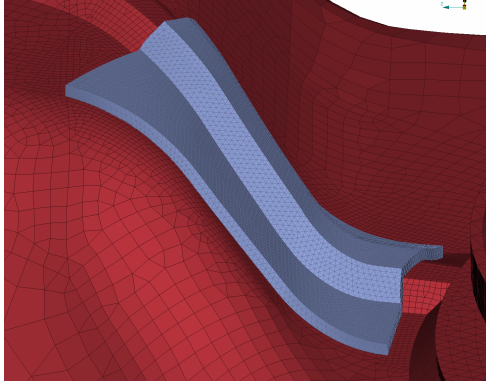


Figure 3.4: *Local zone with a refined solid mesh, surrounded by global zone of shell elements.*

The shell mesh and the solid mesh are not originally connected, so in order to transfer temperatures and displacements it is necessary to couple the two meshes. In the case of displacement coupling, a shell-to-solid coupling was used which constrains the sides of the solid mesh to displace in the same manner as the midsurface of the shell mesh. One issue with this approach is that the stress-strain field at the shell-solid interface may be untrustworthy. The most common solution is to place the interface far away from regions of interest, which was the methodology employed in this investigation. Temperature was coupled by using an extremely large gap conductance, in effect simulating perfect conduction between the two meshes.

3.4 Materials

The exhaust manifold package is made from two austenitic stainless steels, Steel X and Steel Y. In addition to this, the weld seam in region weld A-B uses the filler material Filler X, while the remaining weld seams use the filler material Filler Y. Due to lack of reliable temperature-dependent material data for all the materials, the entire exhaust manifold package, including weld seams, was modelled as having the properties of Steel X. The main limitation of this approach was that it was not possible to examine the effect of material mismatch between the base metal and the weld, which is known to have an effect on the low cycle fatigue life of welds [13].

All of the thermomechanical properties such as expansion coefficient α , thermal conductivity k , specific heat capacity c_p , Young's modulus E , Poisson ratio ν and yield stress σ_y were set to be temperature-dependent. Hardening behaviour was modelled by using the Chaboche elasto-plastic material model [19], which has a non-linear kinematic hardening component and a linear isotropic hardening component. The model parameters were calibrated from half-cycle data at different temperatures using ABAQUS. Half-cycle data means that the stress-strain behaviour is obtained from a monotonic tensile test. It is usually less accurate to use half-cycle data compared to data from a stabilised cycle, since the monotonic stress-strain curve is different from the cyclic stress-strain curve. However, it was only possible to obtain temperature-dependent data from monotonic tensile tests. Fatigue data for Steel X was obtained from the FEMFAT software package [20], where elastic and plastic Coffin-Manson coefficients were available. Temperature dependency was not included in the fatigue data since it was not available.

3.5 Thermal analysis

The thermal analysis was performed as a transient heat transfer analysis divided into three stages: heating, boiling and cooling. Exhaust gas temperature, ambient air temperature and heat transfer coefficients were obtained from CFD simulations performed at VCC. The exhaust gas temperature and ambient air temperature were given as functions of time, while the heat transfer coefficients were constant. The exhaust gas temperatures were applied as film conditions on the inner surfaces of the runners, turbocharger and exit flange. The outer surfaces of these components were then setup to exchange heat through cavity radiation with the surrounding outer shell. Surfaces that would be in contact with the surrounding air were set to exchange heat via convection and radiation with the surrounding. Thermal contacts were modelled using gap conductance with rule-of-thumb values used by VCC. The heat exchange between the cylinder head flanges and the cylinder head was modelled as a cyclic temperature boundary condition with temperatures from a similar analysis performed at VCC. Figure 3.5 shows the points where the maximum and minimum temperature had been previously measured during the thermal shock tests. These values were used to calibrate the thermal analysis.

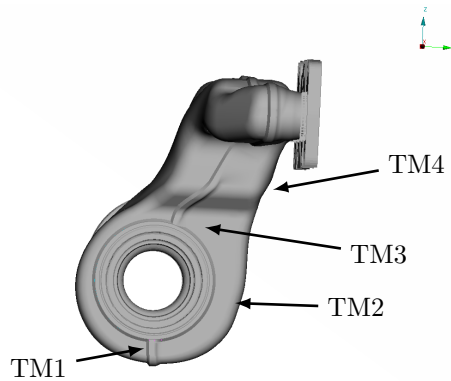


Figure 3.5: *Location of temperature measurement points.*

3.6 Structural analysis

The temperature field from the thermal analysis was fed into the structural analysis. Thus, the full analysis was considered to be a sequentially coupled thermal stress analysis where the temperature field influenced the displacement, but not the other way around. ABAQUS solves these problems by calculating the thermal strain increment associated with the temperature difference over one time step.

Since the cylinder head and the remaining exhaust system were excluded from the analysis, it was necessary to use approximate boundary conditions. The chosen method was to constrain the cylinder head flange surfaces that would be in contact with the cylinder head. In order to validate this approach, data was gathered from a similar simulation performed by a colleague at VCC [21] which included a complete engine model for a similar engine. Figure 3.6 shows the average displacement magnitude of the cylinder head flanges. It can be seen that flange 1 and flange 2, i.e. the outer flanges, have the largest displacement magnitude.

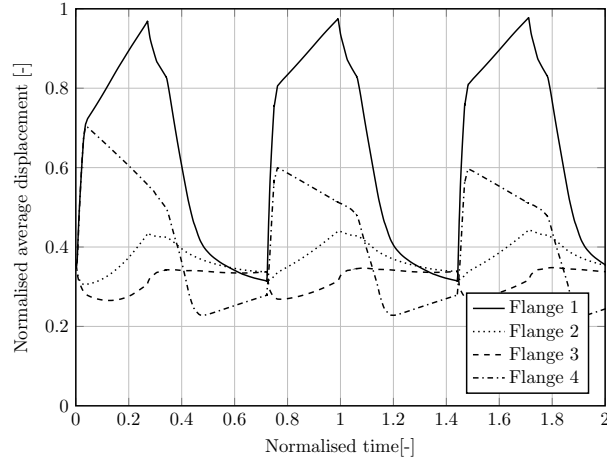
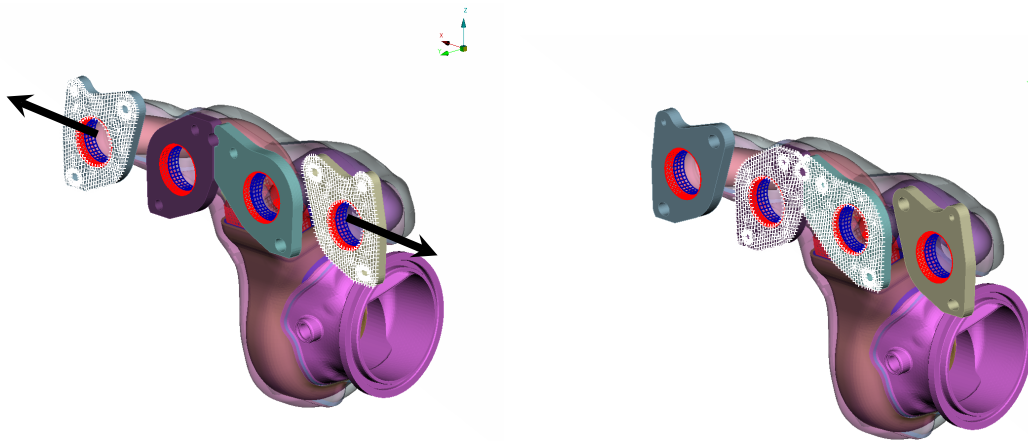


Figure 3.6: Average displacement magnitude on the cylinder head flange surfaces of a similar engine.

In light of the investigation of flange displacement, it was decided to allow movement in the X-direction for the outer flanges, while constraining movement in the Y and Z direction. The inner flanges were completely fixed. Figure 3.7 shows the boundary conditions that were finally implemented.



(a) Nodes allowed to move in the X-direction

(b) Nodes fixed in all directions.

Figure 3.7: Mechanical boundary conditions to eliminate rigid body modes.

3.7 Contacts

Since there were several discrete components that interacted with each other, it was necessary to define contact conditions as shown in Table 3.1.

Table 3.1: Contacts and corresponding properties for thermal and mechanical analyses.

Contact	Thermal interaction	Mechanical interaction
Scroll to exit flange	Thermal conductance	Tie
Runners to lower shell	Thermal conductance	Tie
Lower shell to flanges 1-4	Thermal conductance	Tie
Runners to scroll inlet	-	Tie

Thermal conductance between the runners and the scroll inlet was omitted since both components were approximately the same temperature. The main reason for using a tie condition during the mechanical analysis

was that contact stresses were not of interest. Therefore, it was sufficient to model the behaviour as if the components were tied rigidly. As mentioned earlier in the chapter, it is also necessary to couple shell-to-solid interfaces. This was performed in the same manner as for the global-local model, i.e. to use a shell-to-solid coupling.

4 Fatigue evaluation methodology

This chapter describes the methodology employed to model the welds, in addition to describing the specific procedures used to calculate the fatigue life. It is important to note that the methodology for evaluating fatigue life covers both the weld region and the surrounding base material.

4.1 Weld modelling

The term weld modelling can take on many different meanings, but most common interpretation in the context of fatigue analysis is that it describes how the weld is represented geometrically in the finite element mesh. The geometric description influences the stiffness of the weld, which has an effect on the subsequent displacement field and associated stresses and strains. In addition to this, the geometric description determines the severity of the geometrical discontinuity associated with the weld toe and root. Connected to the geometrical discontinuity, there is so called weld evaluation which governs how the stress-strain field is evaluated in the vicinity of the weld toe or weld root.

4.1.1 Oblique shell elements

For the base model, all welds on the exhaust manifold were modelled using oblique shell elements as illustrated in Figure 4.1. The thickness of the weld elements was set to $\max[t, a]$ where t is the plate thickness and a is the throat size. The throat size is defined as the distance from the surface of the weld to the root of the weld. It can be noted that the stiffness of the weld was not properly modelled since the weld element does not correspond geometrically to the actual weld geometry. Shell elements are based on the midsurface of the actual geometry and correspond geometrically to plates. Therefore, it is not possible to exactly model thick geometries such as pyramids, prisms or spheres. The true three dimensional geometry of a fillet weld can be interpreted as a triangular prism, which means that shell elements are not sufficient. However, modelling welds with oblique shell elements is one of the easiest weld modelling methods available, and was therefore chosen as the base case. Beyond the limitations associated with representing the stiffness, there are also limitations with regard to failure modes and stress concentrations. Using oblique shell elements means that only weld toe failure is captured. Furthermore, the stress concentration at the weld toe is overestimated since the notch has zero radius.

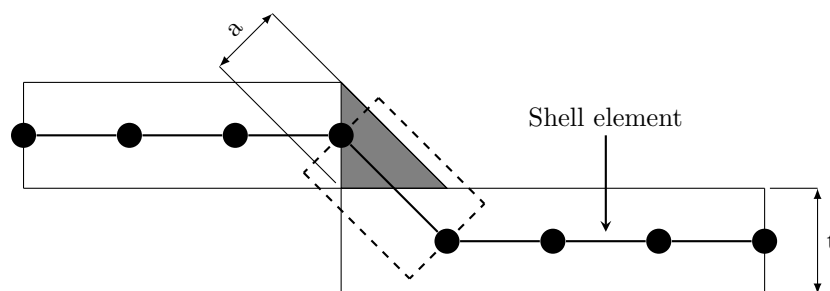


Figure 4.1: Illustration of the weld modelling technique employed for the shell mesh. The dashed line indicates the actual shell geometry with thickness included.

4.1.2 Solid elements

In the global-local model, the weld was represented by quadratic tetrahedral elements. By modelling the weld with solid elements, the stiffness of the weld is more accurately represented. Furthermore, it is possible to model both the weld toe and the weld root. The main limitation of this method is that the model size is dramatically increased. Furthermore, no special modelling technique is applied to the weld toe or weld root which means that they remain singular points in the finite element mesh.

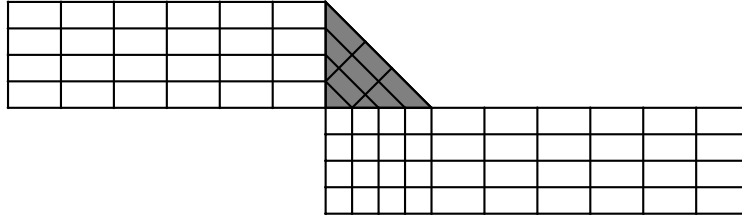


Figure 4.2: *Idealised example of a solid weld mesh.*

4.1.3 Solid elements with effective notch method

Sharp notches as represented by a finite element model do not exist in reality. All sharp corners have some finite radius, and this includes the toe or root of a weld. The effective notch method accounts for this by modelling the weld toe or weld root as a fictitious notch of known size. Plates with thickness above 5 mm are often modelled with a notch radius $\rho = 1$ mm in design codes, while thin plates with thickness below 5 mm use a notch radius of either $\rho = 0.30$ mm or $\rho = 0.05$ mm [22]. The reason for the use of different radii is simply that thinner plates have smaller welds, and therefore smaller toe/root radii. It is important to note that real welds will have variable toe radius since the welding process is highly variable. Therefore, the stress-strain state in the modelled notch must be seen as an idealisation of reality since the actual notch radius may be larger or smaller than the effective notch radius. When it comes to mesh guidelines for the effective notch mesh, the most common approach is to use three elements over the fillet radius in order to properly resolve the geometry and stress gradients. Figure 4.3 shows an idealised mesh for an effective notch model. In reality, it is often difficult and time consuming to construct a structured mesh with hexahedral elements.

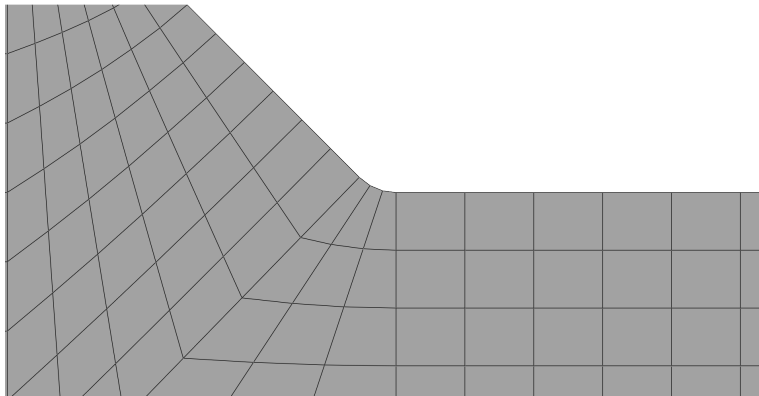


Figure 4.3: *Example of mesh for the effective notch method.*

In this investigation, the geometry of the weld was not ideal and therefore it was not possible to create a structured mesh as previously shown. Instead, the effective notch mesh was created using quadratic tetrahedral elements. Figure 4.4 shows the effective notch mesh used. In total, the local model consists of 314347 elements.

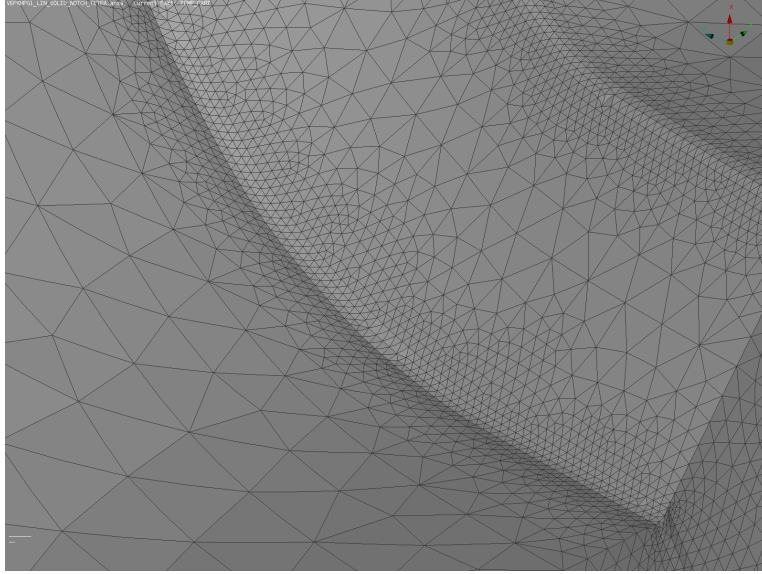


Figure 4.4: *Actual effective notch mesh employed in this investigation.*

4.1.4 Weld evaluation

Weld evaluation deals with how to obtain an accurate stress-strain field in the vicinity of the weld, since the actual stress-strain field will be exaggerated due to the presence of the notch. In this investigation, the traditional methods of using the nominal strain or the structural strain were not applicable since they were not compliant with the chosen damage models. Therefore, the models with sharp notches, i.e the weld model with shell elements and the weld model with solid elements, were evaluated using the actual stress-strain field at the weld toe. Inevitably, this introduced errors to the fatigue life estimation. For the effective notch mesh, the weld toe radius was resolved and therefore the stress-strain field could be obtained directly from the notch.

4.2 Damage models

In order to evaluate fatigue life from a given stress-strain field, it is necessary to quantify damage in terms of the stress-strain state. Damage models may be rooted in theoretical mechanics or they may be purely empirical. However, all of the available damage models depend on model parameters that are obtained from fatigue testing. Therefore, the accuracy of any fatigue assessment is inevitably tied to the confidence level of the model parameters and other material data. In this investigation, two damage models were studied in order to assess their performance with respect to known failure locations and fatigue lives for Exhaust Manifold X.

4.2.1 Coffin-Manson damage model

This investigation uses the Coffin-Manson damage model as the reference model for fatigue life evaluation, due to its prevalence within industry. While it is a prevalent approach for both uniaxial and multiaxial LCF within industry, it must be noted that it is usually a poor approach for weld fatigue [23]. This is due to the fact that welds are particularly sensitive to stresses perpendicular to the weld toe or root. By employing an equivalent stress-strain approach, the importance of directionality is lost. Nonetheless, the model is described by

$$\bar{\varepsilon}_a = \underbrace{\frac{\sigma'_f}{E}(2N_f)^b}_{\bar{\varepsilon}_a^e} + \underbrace{\varepsilon'_f(2N_f)^c}_{\bar{\varepsilon}_a^p} \quad (4.1)$$

where the damage parameter is the equivalent strain amplitude $\bar{\varepsilon}_a$ and σ'_f , ε'_f , b and c are considered model parameters obtained from fitting the model to test data. It is common to use the approximation $\bar{\varepsilon}_a \approx \bar{\varepsilon}_a^p$ when the material is subjected to large plastic deformations. That was the case in this investigation, since the elastic

strain amplitude was nearly negligible in comparison to the plastic strain amplitude. The equivalent plastic strain $\bar{\varepsilon}^p$ is defined as a default variable in ABAQUS [24] as

$$\bar{\varepsilon}^p = \frac{1}{\sigma_Y} \int_0^t \boldsymbol{\sigma} : \dot{\boldsymbol{\varepsilon}}^p dt \quad (4.2)$$

where $\boldsymbol{\sigma}$ is the stress tensor, $\dot{\boldsymbol{\varepsilon}}^p$ is the plastic strain rate tensor¹ and σ_Y is the yield stress. From this, the amplitude $\bar{\varepsilon}_a^p$ may be obtained from

$$\bar{\varepsilon}_a^p = \frac{\bar{\varepsilon}_k^p - \bar{\varepsilon}_{k-1}^p}{4} \quad (4.3)$$

where k denotes the last time step in a cycle and $k - 1$ denotes the first time step in a cycle. The motivation for dividing the difference in equivalent plastic strain over a cycle by four is that $\bar{\varepsilon}^p \geq 0$ and that two reversals occur during a cycle. Since the Coffin-Manson relation includes $2N_f$ in its definition, it would have been faulty to divide the difference by two.

4.2.2 Swith-Watson-Topper damage model

The multiaxial LCF damage model employed in this investigation was the Swith-Watson-Topper (SWT) model. It is a critical plane approach based on the assumption that crack initiation and propagation will occur due to normal strain on a critical plane with influence from the maximum normal stress during a cycle. Typically cracks initiate due to shear stresses on the microscale and then propagate due to normal stresses. However, welded joints with a high geometrical discontinuity always have some initial cracks or crack-like inclusions which means that crack initiation can be considered to have already occurred before any loading is applied [23]. Therefore, the SWT model may be a suitable choice to estimate the number of cycles until failure due to its reliance on normal stresses and strains on a critical plane. Furthermore, the material parameters are identical to the Coffin-Manson model, which simplifies comparison. Equation (4.4) shows the fatigue life equation for the SWT model

$$\sigma_{n,max} \frac{\Delta\varepsilon_n}{2} = \frac{(\sigma'_f)^2}{E} (2N_f)^{2b} + \sigma'_f \varepsilon'_f (2N_f)^{b+c} \quad (4.4)$$

where $\sigma_{n,max}$ is the maximum normal stress on the plane during a cycle and $\Delta\varepsilon_n$ is the normal strain range on the plane. In principle, the SWT model is an extension of the Coffin-Manson equation with influences from the mean stress through $\sigma_{n,max}$. The main difference is that the SWT model is evaluated on all possible material planes to find the minimum fatigue life. The variation of the fatigue life with respect to the damage parameter $\sigma_{max}\varepsilon_a$ for all planes for the material Steel X can be seen in Figure 4.5

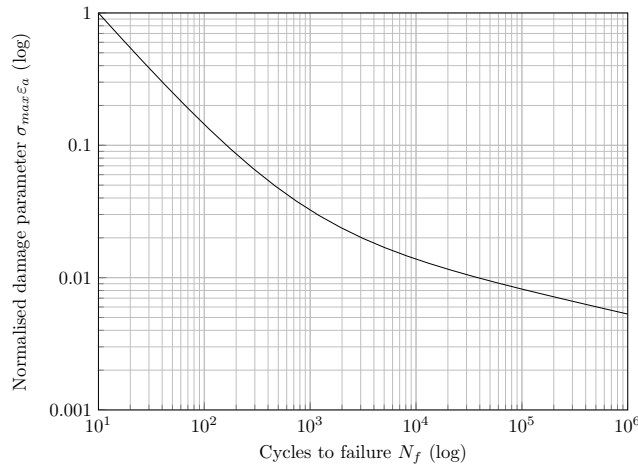


Figure 4.5: SWT curve for the material Steel X. Curve normalised with respect to the damage parameter value at $N_f = 10$

The critical plane search is based on generating potential crack planes and calculating the normal and shear stress-strain on the plane. Figure 4.6 shows an example of a crack plane with a rotated frame $x'y'z'$,

¹Both the stress tensor and plastic strain rate tensor are second order tensors.

where the plane is defined by its normal vector $\tilde{\mathbf{n}}(\theta, \phi)$. As can be seen, the normal component acts along the z' axis while the shear components act along both the x' and y' axis. That means that during a cycle, the normal stress-strain will have a fixed direction but varying magnitude. Therefore, it is trivial to calculate the normal stress-strain range. The shear stress-strain will however vary along two axes during a cycle and traces a closed path on the crack plane over a cycle. Common procedures for evaluating the amplitude of the shear stress-strain include finding the longest chord or finding the minimum circle that encloses the path. These methods increase the computational cost since they require finding the optimal solution to a min-max problem. In this investigation, it was not necessary to include them since the SWT model only considers normal stress and strain on the plane.

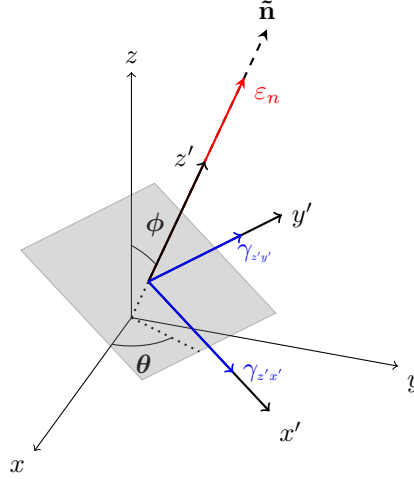


Figure 4.6: Example of a critical plane with a rotated frame $x'y'z'$. The normal and shear components on the plane are shown.

Computing the normal and shear contributions on the plane requires knowledge of the rotation matrix \mathbf{A} associated with the two rotations. It is defined by

$$\mathbf{A} = \begin{bmatrix} \cos \theta \sin \phi & \sin \theta \sin \phi & \cos \phi \\ -\sin \theta & \cos \theta & 0 \\ -\cos \theta \cos \phi & -\sin \theta \cos \phi & \sin \phi \end{bmatrix} \quad (4.5)$$

where the components are denoted a_{ij} . The normal stress on the plane can be computed according to [8] as

$$\sigma_n = \sigma_{xx}a_{11}^2 + \sigma_{yy}a_{12}^2 + \sigma_{zz}a_{13}^2 + 2(\tau_{xy}a_{11}a_{12} + \tau_{xz}a_{11}a_{13} + \tau_{yz}a_{13}a_{12}) \quad (4.6)$$

where the stress components σ_{ij} are from the global reference frame xyz . In a similar fashion, the normal strain may be computed as

$$\varepsilon_n = \varepsilon_{xx}a_{11}^2 + \varepsilon_{yy}a_{12}^2 + \varepsilon_{zz}a_{13}^2 + 2(\varepsilon_{xy}a_{11}a_{12} + \varepsilon_{xz}a_{11}a_{13} + \varepsilon_{yz}a_{13}a_{12}) \quad (4.7)$$

It is important to note that most finite element codes output the engineering shear strain $\gamma_{ij} = \varepsilon_{ij} + \varepsilon_{ji}$ for $i \neq j$. By using the symmetry of the strain tensor ε_{ij} , it is possible to compute the proper shear strains that are required by Equation (4.7). The critical plane search and SWT damage model was implemented as a Python script that interacted with the ABAQUS output database to calculate and plot the number of cycles to failure for each element. The algorithm for the critical plane search is presented in Algorithm 1. It is based on finding the plane with the largest damage parameter $\sigma_{n,max} \frac{\Delta \varepsilon_n}{2}$ and therefore the lowest fatigue life N_f . Since each element may have multiple integration points, the integration point where the stress and strain tensors had the largest norm was chosen. This was mainly to reduce the computational time required to perform a critical plane search.

Algorithm 1 Critical plane algorithm for one element

Input: $\boldsymbol{\sigma}(t), \boldsymbol{\varepsilon}(t)$ **Output:** $N_{f,min}$ **for all** (Φ, θ) **do** Compute rotation matrix $\mathbf{A}(\theta, \phi)$ **for** $t = 0$ **to** T **do**

$$\sigma_n(t) = \sigma_{xx}a_{11}^2 + \sigma_{yy}a_{12}^2 + \sigma_{zz}a_{13}^2 + 2(\tau_{xy}a_{11}a_{12} + \tau_{xz}a_{11}a_{13} + \tau_{yz}a_{13}a_{12})$$

$$\varepsilon_n(t) = \varepsilon_{xx}a_{11}^2 + \varepsilon_{yy}a_{12}^2 + \varepsilon_{zz}a_{13}^2 + 2(\varepsilon_{xy}a_{11}a_{12} + \varepsilon_{xz}a_{11}a_{13} + \varepsilon_{yz}a_{13}a_{12})$$

end for

$$\Delta\varepsilon_n = \max_t[\varepsilon_n(t)] - \min_t[\varepsilon_n(t)]$$

$$\sigma_{n,max} = \max_t[\sigma_n(t)]$$

 Compute $\sigma_{n,max} \frac{\Delta\varepsilon_n}{2}$ **end for**Find critical plane (θ, ϕ) where $\sigma_{n,max} \frac{\Delta\varepsilon_n}{2}$ is largestCompute the minimum fatigue life N_f with the SWT model

While [8] states that the plane angle $\phi = 0^\circ$ will always be the dominant crack plane for the SWT model, both ϕ and θ were varied from 0° to 360° . This is due to the fact that it was difficult to obtain the correct orientation of an arbitrary element by using the built-in ABAQUS scripting functionality. For a shell element, it is trivial to find the current orientation since the orientation will be defined by the single normal vector of the shell element. The same is not true for a tetrahedral element since it has several normal vectors. Therefore, it was necessary to search all possible planes since the plane corresponding to $\phi = 0^\circ$ was unknown a priori. However, this did not significantly impact the performance of the critical plane search since the additional time required to search more planes was negligible compared to the time required to extract a stress-strain time history for an element.

4.2.3 Mean stress effects

Due to the welding process, welds tend to have tensile residual stresses which may reduce the fatigue life. The negative effect of tensile residual stresses on the fatigue life is well documented for HCF, while the effect on LCF has been shown to be marginal in some cases due to stress relaxation [25]. Despite this, it was considered worthwhile to examine the effects of tensile residual stresses by considering them a mean stress effect. In principle, a tensile mean stress aids in opening a crack and makes it easier for the crack to propagate through the material. In order to incorporate the effect of mean stresses in the fatigue life prediction, the Coffin-Manson model was modified by using the modified Morrow correction [3]. The SWT damage model includes mean stresses within the term $\sigma_{n,max}$, but it was not possible to easily modify the term to include artificial mean stresses as with the modified Morrow correction. Therefore, the study of residual stresses was limited to the Coffin-Manson model. The modified Morrow mean stress correction is defined by

$$\varepsilon_a = \frac{\sigma'_f}{E} \left(1 - \frac{\sigma_m}{\sigma'_f} \right) (2N_f)^b + \varepsilon'_f (2N_f)^c \quad (4.8)$$

where the elastic part of the Coffin-Manson equation is modified by the term σ_m/σ'_f , where σ_m is the mean stress. The reason for not modifying the plastic term is that mean stress effects have a reduced effect at relatively short fatigue lives [3]. This investigation did not simulate the actual residual stress field in the vicinity of the weld. Instead, a simplified approach was used whereby the mean stress was assumed to be $\sigma_m = \sigma_Y/2$. This corresponds to a pulsating stress state ($R = 0$) where the maximum stress is limited by the yield limit σ_Y , as exemplified in Figure 4.7

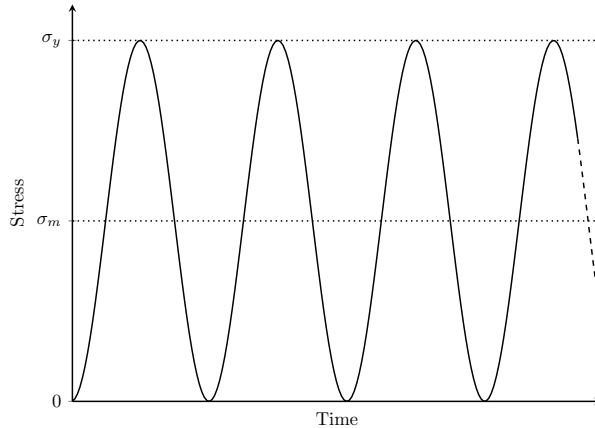


Figure 4.7: *Example of constant amplitude pulsating stress with mean stress $\sigma_m = \sigma_y/2$*

This is not true to reality, but the main goal of the approach was to examine whether a tensile mean stress had any effect at all for the fatigue life of the exhaust manifold. Therefore, it was sufficient to consider a mean stress that was relatively high, but not necessarily accurate to the actual residual stress state.

4.3 Statistical analysis of fatigue data

Fatigue lives from experimental testing are always subject to large variations due to material defects, imperfect test conditions and other factors. For the thermal shock test, the engine is subjected to a set amount of cycles and any cracks that occur are recorded together with the amount of cycles to crack initiation. Each test constitutes a sample, where the pertinent parameter is denoted x . With a given number of samples, it is possible to calculate the sample mean \bar{x} as

$$\bar{x} = \frac{1}{n} \sum_{i=1}^n x_i \quad (4.9)$$

where n denotes the number of samples. The variability in the samples is typically measured with the sample standard deviation s_x , defined as

$$s_x = \sqrt{\frac{\sum_{i=1}^n (x_i - \bar{x})^2}{n - 1}} \quad (4.10)$$

From these two measures, it is possible to define the coefficient of variation δ_x as

$$\delta_x = \frac{s_x}{\bar{x}} \quad (4.11)$$

which is a dimensionless measure of the uncertainty in the value of x . According to [3], the coefficient of variation is convenient since its value is typically constant for a given property, e.g. yield strength or number of cycles to failure. It was suggested by [26] that $\delta_x = 23\%$ for austenitic stainless steels across all fatigue lives, and that δ_x varies between $\delta_x = 18\%$ and $\delta_x = 29\%$ for low cycle fatigue lives across a wide range of materials. Based on this information, the value $\delta_x = 25\%$ was used in this investigation.

According to the responsible system engineer at VCC [27], the weld seams typically experience crack initiation in the weld toe between $N_f = 0.6$ and $N_f = 0.7$ cycles which would result in a sample mean $\bar{x} = 0.65$. The fatigue lives were normalised with respect to the maximum number of cycles in a thermal shock test. While the actual variation was unknown, it was possible to estimate the sample standard deviation by using the previous value for δ_x . The sample standard deviation for the experimental testing was estimated to

$$s_x = \delta_x \bar{x} = 0.1625 \quad (4.12)$$

Any numerical fatigue life estimate that falls within one sample standard deviation can be considered to be within the margin of error for the experimental testing.

5 Results

The results are presented in sequential order, beginning with the thermal analysis and finishing with the fatigue life analysis. All the results are normalised in order to preserve confidentiality. For the thermal analysis and the structural analysis, the results are normalised with the maximum value that was obtained during the simulation. The fatigue analysis is normalised with the maximum number of cycles in a thermal shock test.

5.1 Thermal analysis

Figure 5.1 shows the temperature as a function of time for different parts of the exhaust manifold. The largest temperature difference ΔT corresponds to approximately $0.57T_g$ where T_g is the maximum exhaust gas temperature. The latter cycles are subjected to a lower temperature differential since the engine is not cooled to room temperature between heating cycles.

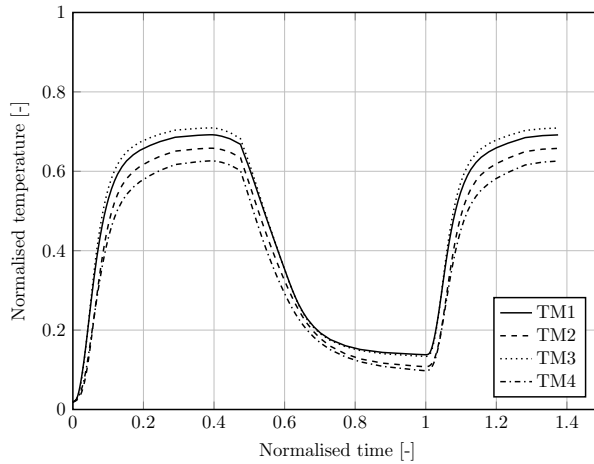


Figure 5.1: *Temperature history throughout 1.5 thermal cycles in chosen material points on the upper shell, lower shell, scroll and weld.*

The obtained temperature field from the thermal analysis was calibrated against experimental data that was available from testing made by VCC. Table 5.1 shows a comparison of temperature values from the experiment and from the thermal FEA. It can be seen in general, FEA overestimates the maximum temperature and underestimates the minimum temperature, leading to a larger temperature difference. The correlation could be considered satisfactory considering that CFD mapping was not used when applying film coefficients and gas temperatures.

Table 5.1: Comparison of maximum and minimum temperatures between experiment and FEA. Results are normalised with the maximum exhaust gas temperature T_g .

Measurement point	Exp. T_{\max}/T_g	Exp. T_{\min}/T_g	FEA T_{\max}/T_g	FEA T_{\min}/T_g
TM1	0.67	0.09	0.69	0.14
TM2	0.64	0.17	0.65	0.11
TM3	0.73	0.11	0.71	0.13
TM4	0.61	0.14	0.63	0.10

Figure 5.2 shows the nodal temperature distribution from an outside perspective. It can be seen that there is a fairly significant temperature gradient in the outer shell for the cold state, while the temperature distribution during the hot state is fairly uniform.

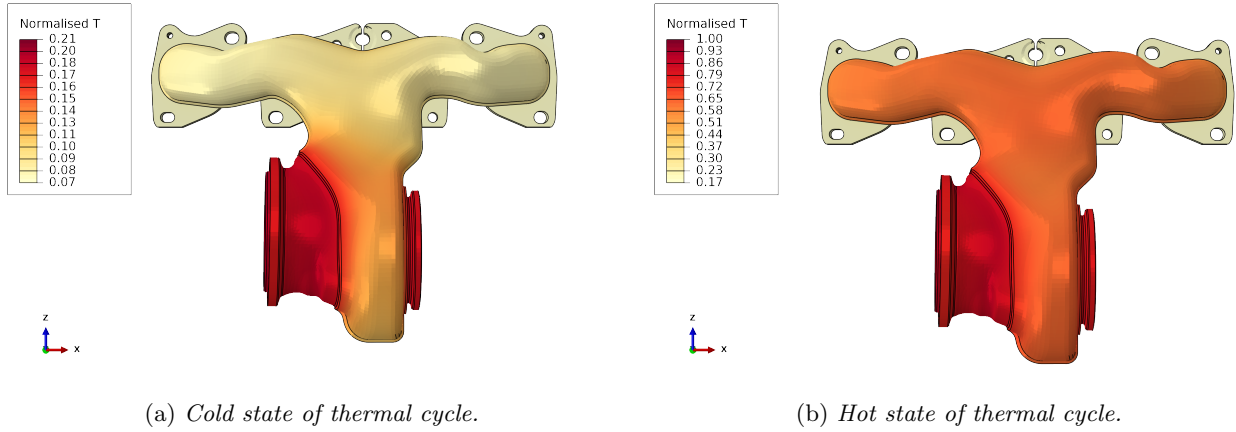


Figure 5.2: Outer view of the nodal temperature distribution for the cold and hot state of the thermal cycle. Results normalised with maximum exhaust gas temperature T_g .

Figure 5.3 shows the nodal temperature distribution inside the exhaust manifold housing. It can be seen that the runners and the scroll are significantly hotter than the surrounding outer shell.

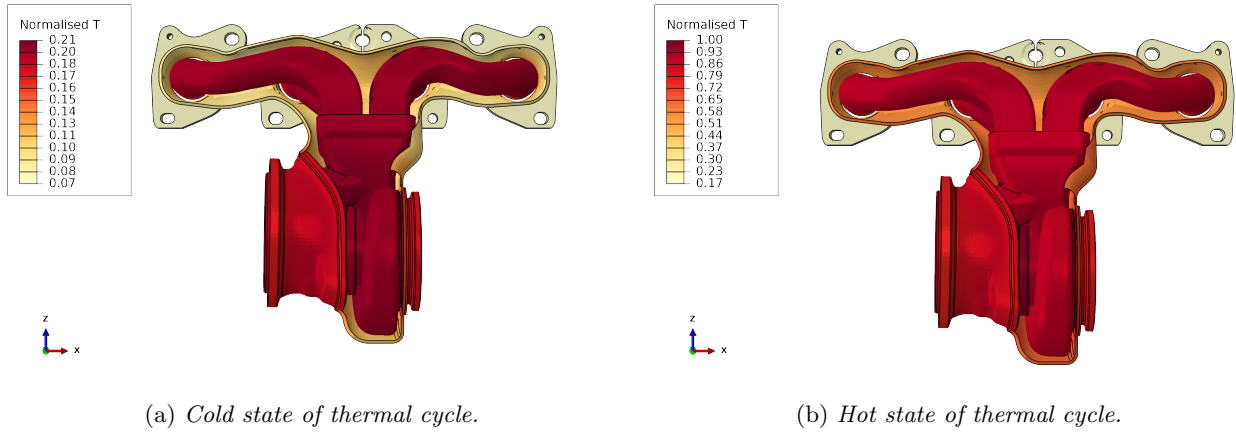


Figure 5.3: Inner view of the nodal temperature distribution for the cold and hot state of the thermal cycle. Results normalised with maximum exhaust gas temperature T_g .

When comparing the temperature fields to test data and old simulations performed at VCC, it was deemed that the thermal analysis could be considered accurate enough for use in a structural analysis.

5.2 Structural analysis

The structural analysis formed the basis for the fatigue analysis and the expected result was a stabilized constant amplitude plastic cycle from which to compute fatigue life according to the chosen damage models. Figure 5.4 shows the ratio of shear strain γ_{xy} to normal strain for two normal components ε_{xx} and ε_{xy} . It can be clearly seen that the strain state is non-proportional, which highlights the need for a critical plane analysis when evaluating the fatigue life.

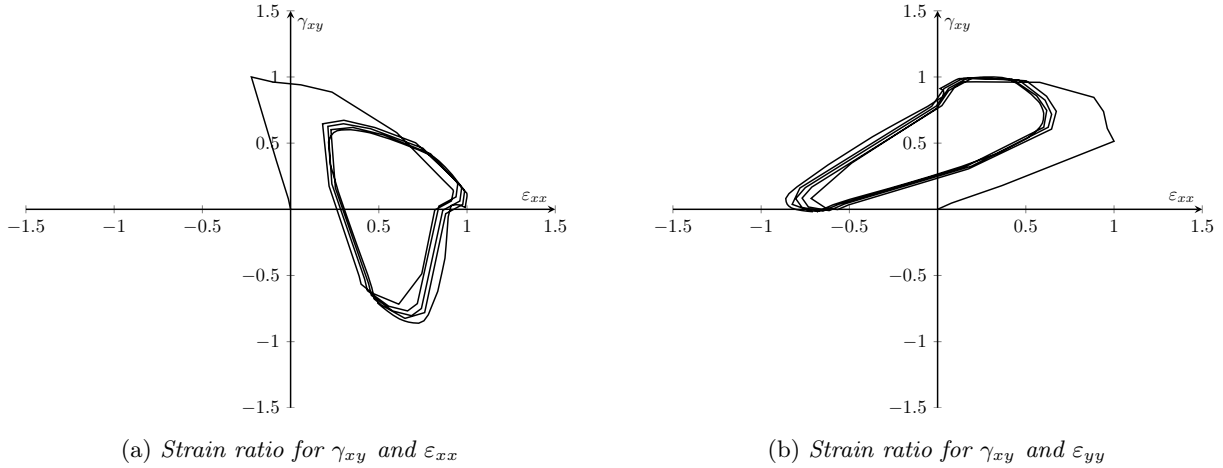


Figure 5.4: Normalised strain ratios in a critical element in the region weld A-B.

Figure 5.5 shows the cyclic stress-strain behaviour of one element in the region weld A-B over 5 thermal cycles. It can be seen that the behaviour stabilises quickly, showing virtually no signs of ratcheting. Since the element in question resides in one of the most stressed locations, the cyclic behaviour is considered to be representative of the remaining elements since elements that experience lower loading will stabilise faster.

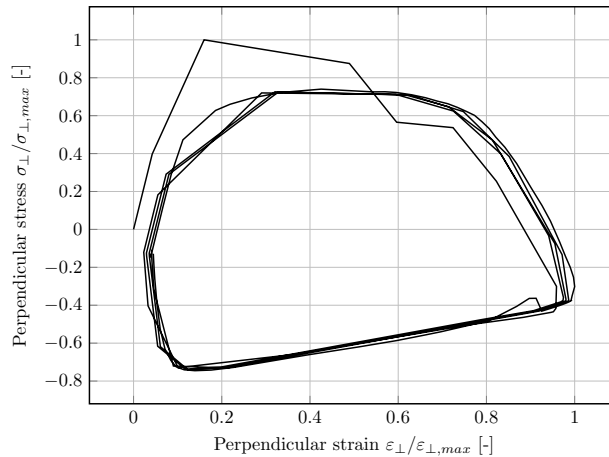


Figure 5.5: Cyclic stress-strain behaviour over 5 thermal cycles for a critical element in the weld toe in region weld A-B. The stresses and strains are perpendicular to the weld toe.

5.3 Fatigue

Fatigue life results are scaled by the maximum amount of cycles in the thermal shock test. In other words, a fatigue life value of 1 corresponds to the full amount of cycles in the test. The fatigue results can therefore be interpreted as safety factors against fatigue. Figure 5.6 shows a summary of the fatigue life results and compares the different meshes and fatigue models. As can be seen, the fatigue life estimates for the shell mesh fall within the margin of error for the experimental fatigue life. In contrast, both the solid mesh and the notch mesh fall outside the margin of error.

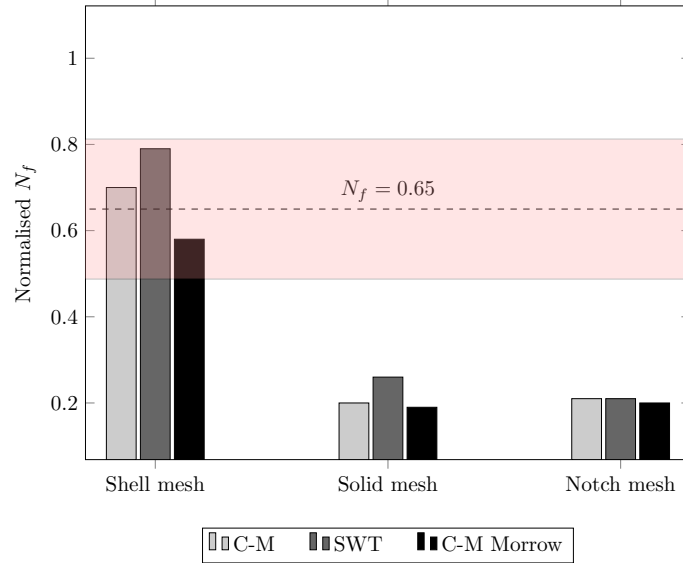


Figure 5.6: Summary of the fatigue life results. C-M denotes the Coffin-Manson method. The dashed line denotes the mean experimental fatigue life. The band indicates one sample standard deviation given $\delta_x = 25\%$.

It can be noted that the solid mesh and the notch mesh provide conservative fatigue life estimates regardless of the chosen damage model. While the presented graph in Figure 5.6 summarises the fatigue life estimates, it does not indicate the possible fatigue hot spots. Therefore, the following sections provide contour plots that show where the different meshes and damage models predict fatigue failure.

5.3.1 Oblique shell elements

Figure 5.7 shows the fatigue life predictions for the model where the weld was modelled using oblique shell elements. It can be seen that the Coffin-Manson model indicates failure in the vicinity of the upper weld toe while the SWT model predicts the failure location to be the lower weld toe. Both the Coffin-Manson model and the SWT model predict similar fatigue life estimates that correspond well to the experimental values.

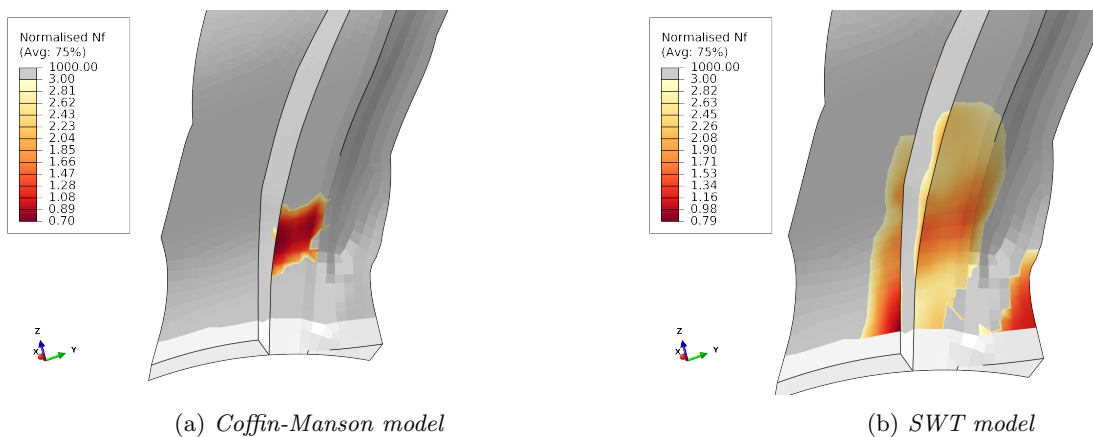


Figure 5.7: Fatigue life estimates for the shell weld mesh. Grey and white areas indicate fatigue lives beyond the scope of the thermal shock test.

5.3.2 Solid elements

Figure 5.8 shows the fatigue life estimation for the solid weld mesh when using the Coffin-Manson damage model and the SWT model. As can be seen, the SWT model predicts two possible fatigue failure locations: the lower weld toe and a larger region near the upper weld toe. In contrast, the Coffin-Manson model does not

predict failure from the lower weld toe. The fatigue life estimates for both models are conservative compared to experimental values between $N_f = 0.6$ and $N_f = 0.7$.

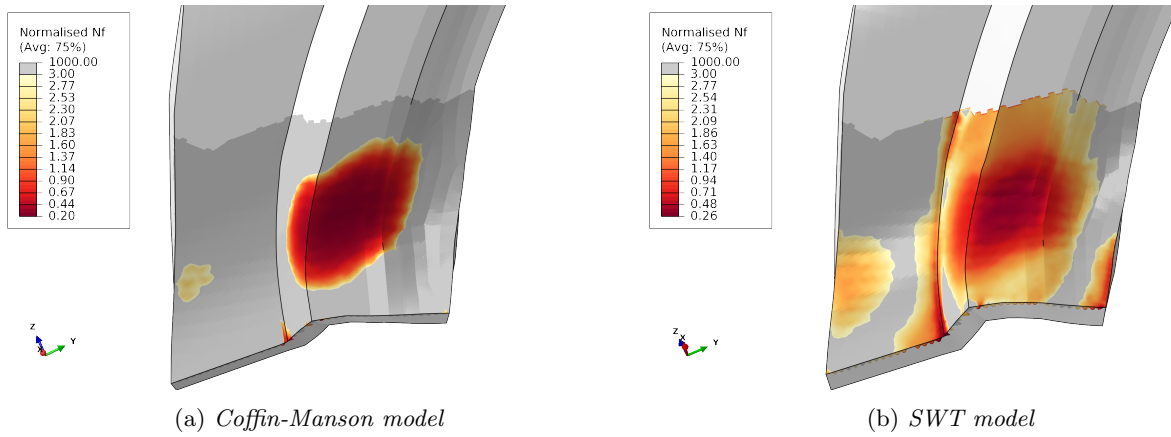


Figure 5.8: Fatigue life estimates for the solid weld mesh.

5.3.3 Solid elements with effective notch method

Figure 5.9 shows the fatigue life estimates for the effective notch method. As can be seen, both models predict failure from the lower weld toe. The fatigue life estimates are conservative and similar to the solid mesh without notch modelling.

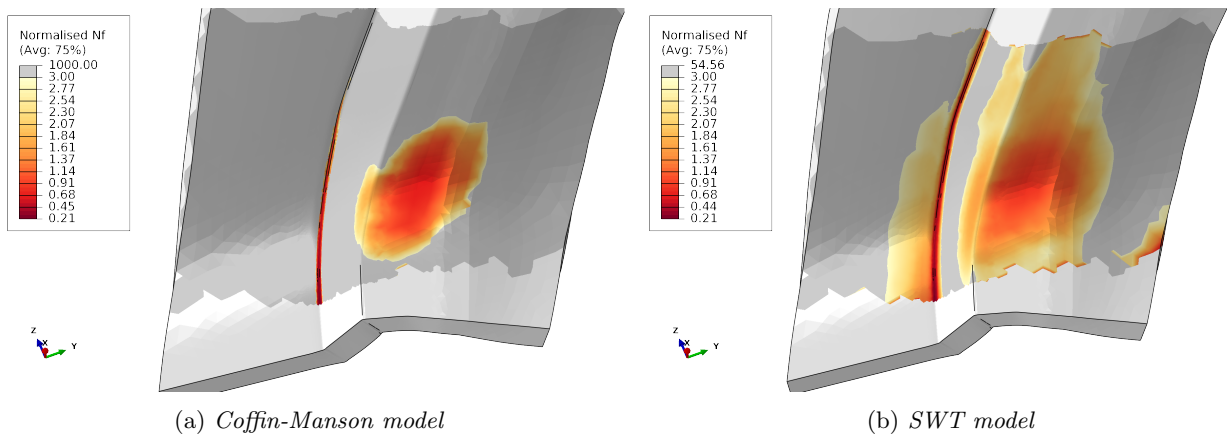


Figure 5.9: Fatigue life estimates for the effective notch mesh.

5.3.4 Mean stress effects

Figure 5.10 shows the fatigue life estimate for the shell mesh when using the Coffin-Manson model together with the modified Morrow correction. It can be seen that the estimated fatigue life is decreased by 17.4% compared to the regular Coffin-Manson model. It is important to note that the zone with the most fatigue damage is extended compared to the Coffin-Manson model without the modified Morrow correction.

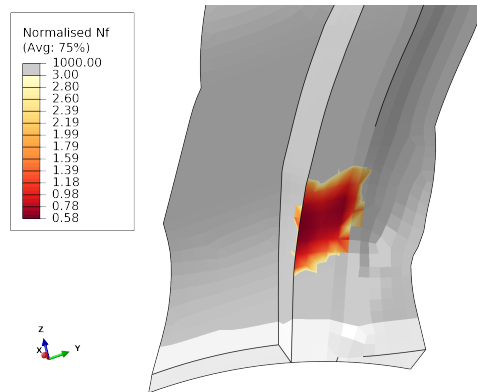


Figure 5.10: *Fatigue life estimate for the shell mesh when using Coffin-Manson with modified Morrow correction.*

Figure 5.11 shows the estimated fatigue life estimate for the solid mesh when using the Coffin-Manson model together with the modified Morrow correction. Compared to the non-modified Coffin-Manson model, the fatigue life estimate is reduced by 8.7%. As with the shell mesh, the zone with the highest fatigue damage is slightly extended.

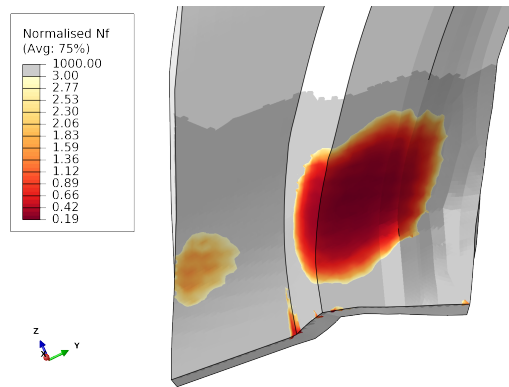


Figure 5.11: *Fatigue life estimate for the solid mesh when using Coffin-Manson with modified Morrow correction.*

Figure 5.11 shows the estimated fatigue life for the effective notch mesh when using the Coffin-Manson model together with the modified Morrow correction. Compared to the non-modified Coffin-Manson model, the fatigue life estimate is reduced by 4.8%. As with both the shell mesh and the solid mesh, the zone with the fatigue damage is extended slightly.

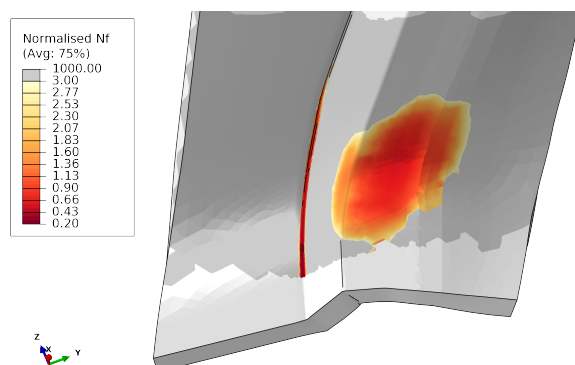


Figure 5.12: *Fatigue life estimate for the notch mesh when using Coffin-Manson with modified Morrow correction.*

6 Discussion

Results from the thermal analysis show good correspondence to measured temperature values in selected points. Correlating temperature fields to experimental data is notoriously difficult, since it is generally not possible to measure the temperature in every material point. Therefore, the spatial variation of the temperature is generally not captured when measuring the temperature. Consequently, the simulated temperature may correspond to the measured temperature in the selected points, but there is no information about the variation between the measured points. However, considering the close correspondence in the selected points, the thermal analysis was likely sufficiently accurate. As for the structural analysis, it was shown that the thermal loading constituted non-proportional loading which justified the use of a critical plane approach. The overall cyclic behaviour was stabilised which was the expected outcome of the structural analysis. There was no experimental correlation for the structural analysis, but the correlation of the thermal analysis can be considered sufficient since the loading was purely thermal.

The results from the fatigue analysis show that the critical plane approach with the SWT model gives a more conservative fatigue life estimate than using the Coffin-Manson model with an equivalent strain approach. The results from the shell mesh corresponds best to the experimental mean fatigue life $N_f = 0.65$. In contrast, both the solid meshes suggest that fatigue failure occurs beyond one standard deviation of the mean fatigue life. Therefore, the fatigue life estimates from the solid meshes are less likely to be reliable. When using shell elements, the predicted failure location is not the same for the SWT model and the Coffin-Manson model. The fatigue failure locations for the SWT model and the Coffin-Manson model do however correspond when using solid elements, which could indicate mesh sensitivity since the solid mesh without notch treatment was finer than the shell mesh. Weld toe failure is only specifically indicated when using the effective notch method. In theory, the solid mesh without notch treatment should also indicate weld toe failure since the weld toe notch is sharper.

All of the studied meshes and models indicate failure in the vicinity of the weld toe, but it is only the effective notch method that accurately specifies the failure to be exactly in the weld toe. Since the experimental evidence clearly indicates weld toe failure, it is likely that it is necessary to resolve the notch in order to capture this phenomena. Regarding the fatigue life estimates, it is difficult to draw any conclusions since the experimental data can be considered sparse at best. There is also considerable spread in the experimental fatigue lives according to the system engineer, although it was not possible to specify the magnitude of the spread. In future investigations, it is imperative that the FEA is accompanied by rigorous experimental testing with adequate documentation.

Including weld residual stresses as a mean stress effect seems to be largely irrelevant at the studied fatigue lives since they fall below the transition life of Steel X. It is more relevant for the studied shell mesh since the estimated fatigue life was higher, but since the shell mesh exhibits some unexpected behaviour, the mean stress effect should be viewed with some cautiousness. It may be useful to include the residual stresses as a mean stress effect for materials where the transition life falls within the scope of the thermal shock test. In order to validate this method, some further investigations should be performed to evaluate the magnitude of the residual stress after the welding process. In addition, the residual stresses should be added to the critical plane model in order to determine the influence of residual stresses for the critical plane approach.

6.1 Error sources

The fatigue life estimates are ultimately dependent on a number of factors that have more or less influence. For example, the temperature loads from the thermal analysis have a significant effect on the stress-strain field. Even a small error in the temperature loads may shift the fatigue life estimates by an order of magnitude. On the same note, the boundary conditions in the structural analysis will also affect the stress-strain field significantly during a thermal stress analysis. The fatigue model parameters were obtained from the software FEMFAT, but the actual source for the experimental data is not known. Since the fatigue life estimates depend greatly on the model parameters, it would benefit the analysis to perform further simulations with different fatigue model parameters.

7 Conclusions

The results show that the critical plane approach and the equivalent strain approach give similar fatigue life estimates, although the critical plane approach was slightly more conservative. It is possible that different critical plane damage models will yield more accurate results. The comparison between different modelling techniques indicate that it is necessary to resolve the weld toe notch in order to accurately capture the failure location. Shell elements come closest to predicting the number of cycles to failure, but there is substantial uncertainty with regards to mesh sensitivity for the shell mesh. Weld residual stresses do not seem to affect the fatigue life estimates. However, it is important to note that the effect of the modified Morrow mean stress correction depends on the proximity to the transition life of the material. The accuracy of the predicted fatigue lives should be viewed with caution since more experimental correlation is needed. While the standard deviation of the experimental sample mean was calculated, it is important to know the actual variation of the experimental fatigue lives in order to draw conclusions about which fatigue damage model or weld modelling method is most accurate.

7.1 Recommendations

Further studies should be performed with other critical plane models such as Fatemi-Socie [10], Brown-Miller [11] among others. It is vital to do this since critical plane models are based on assumptions of the crack initiation and propagation behaviour, which is dependent on the material. It would also be interesting to study the effect of creep on the fatigue life of the exhaust manifold. However, it is necessary to first examine whether it is possible to combine a critical plane approach with creep damage.

If further studies are conducted, efforts should be made to increase the performance of the algorithm for extracting stress-strain time histories from the output file. No matter how accurate the model may be, it should also be industrially viable with regard to computational speed. It may also be interesting to develop a smarter algorithm that evaluates the local stress-strain state and determines whether to employ a uniaxial or a multiaxial damage model. Other improvements would be to allow the user to choose a multiaxial damage model depending on the chosen material.

Bibliography

- [1] Beta CAE. ANSA Pre-processor, Version 17.1.2. <https://www.beta-cae.com/ansa.htm>. Accessed: 2018-04-18.
- [2] Dassault Systèmes. Abaqus/Standard, Version 2017. <https://www.3ds.com/products-services/simulia/products/abaqus/>. Accessed: 2018-04-18.
- [3] Norman E. Dowling. *Mechanical Behavior of Materials*. Pearson, 4th edition, 2012.
- [4] Niels Saabye Ottosen and Hans Petersson. *Introduction to the Finite Element Method*. Prentice Hall, 1992.
- [5] Kenneth Runesson. Constitutive modelling of engineering materials - Theory and computation - The Primer. Lecture notes, Department of Applied Mechanics, Chalmers University of Technology, 2006.
- [6] Anders Ekberg. Multiaxial fatigue edition 5.2. Department of Applied Mechanics, Chalmers University of Technology, Report 2012:02, 2016.
- [7] eFatigue - Multiaxial strain-life technical background. <https://www.efatigue.com/multiaxial/background/strainlife.html>. Accessed: 2018-04-07.
- [8] Darrell F. Socie and Gary B. Marquis. *Multiaxial Fatigue*. Society of Automotive Engineers, 2000.
- [9] R.N Smith, P. Watson, and T.H. Topper. A stress-strain parameter for the fatigue of metals. *Journal of Materials*, 5(4):149–166, 1988.
- [10] Ali Fatemi and Darrell F. Socie. A critical plane approach to multiaxial fatigue damage including out-of-phase loading. *Fatigue and Fracture of Engineering Materials and Structures*, 11(3):767–778, 1970.
- [11] M.W. Brown and K.J. Miller. A theory for fatigue under multiaxial stress-strain. In *Proceedings of the Institute of Mechanical Engineers*, volume 187, pages 745–756, 1973.
- [12] Adolf Hobbacher. *Recommendations for fatigue design of welded joints And components*. International Institute of Welding, Paris, France, 2003.
- [13] Kawin Saiprasertkit, Takeshi Hanji, and Chitoshi Miki. Fatigue strength assessment of load-carrying cruciform joints with material mismatching in low- and high-cycle fatigue regions based on the effective notch concept. *International Journal of Fatigue*, 40:120–128, 2012.
- [14] Pingsha Dong, Xianjun Pei, Shizhu Xing, and Myunghyun Kim. A structural strain method for low-cycle fatigue evaluation of welded components. *International Journal of Pressure Vessels and Piping*, 119:39–51, 2014.
- [15] Pingsha Dong. A robust structural stress method for fatigue analysis of offshore/marine structures. *Journal of Offshore Mechanics and Arctic Engineering*, 127:68–74, 2005.
- [16] Heikki Remes. Strain-based approach to fatigue crack initiation and propagation in welded steel joints with arbitrary notch shape. *International Journal of Fatigue*, 52:114–123, 2013.
- [17] Kimiya Hemmesi, Majid Farajian, and Ali Fatemi. Application of the critical plane approach to the torsional fatigue assessment of welds considering the effect of residual stresses. *International Journal of Fatigue*, 101:271–281, 2017.
- [18] Giuseppe Marulo, Francesco Frenzo, Leonardo Bertini, and Ali Fatemi. On the application of a critical plane approach to the life assessment of welded joints. *Procedia Engineering*, 213:448–458, 2018.
- [19] Jean-Louis Chaboche. A review of some plasticity and viscoplasticity constitutive theories. *International*

Journal of Plasticity, 24:1642–1693, 2008.

- [20] Magna International Inc. FEMFAT, Version 5.2, Accessed April 22, 2018. <https://femfat.magna.com/>.
- [21] Carl Sandström. Personal communication. Gothenburg, March 15, 2018.
- [22] Thomas Bruder, Klaus Störzel, Jörg Baumgartner, and Holger Hanselka. Evaluation of nominal and local stress based approaches for the fatigue assessment of seam welds. *International Journal of Fatigue*, 34:86–102, 2012.
- [23] Åsa Eriksson, Anna-Maria Lignell, Claes Olsson, and Hans Spennare. *Weld evaluation using FEM*. Industrilitteratur AB, 2003.
- [24] Dassault Systèmes. Abaqus Analysis User’s Guide, Version 6.16. <https://www.3ds.com/products-services/simulia/products/abaqus/>. Accessed: 2018-04-11.
- [25] B. Levieil, F. Bridier, C. Doudard, D. Thevenet, S. Calloch, and A. Ezanno. Numerical simulation of low-cycle fatigue behavior of welded joints for naval applications: influence of residual stresses. *Welding in the World*, 61:551–561, 2017.
- [26] P.H. Wirsching. Statistical summaries of fatigue data for design purposes. Technical report, Arizona University, Department of Aerospace and Mechanical Engineering, 1983. <https://ntrs.nasa.gov/search.jsp?R=19830021460>.
- [27] Lena Johansson. Personal communication. Gothenburg, April 10, 2018.